Two-dimensional multi-level strain estimation for discontinuous tissue

Hairong Shi and Tomy Varghese

Department of Medical Physics, The University of Wisconsin-Madison, Madison, WI 53706, USA

E-mail: tvarghese@wisc.edu

Abstract

A large number of the strain estimation methods presented in the literature are based on the assumption of tissue continuity that establishes a continuous displacement field. However, in certain locations in the body such as the arteries *in vivo* scanning may produce displacement fields that are discontinuous between the two walls of the artery. Many of the displacement or strain estimators fail when the displacement fields are discontinuous. In this paper, we present a new 2D multi-level motion or displacement tracking method for accurate estimation of the strain in these situations. The final high-resolution displacement estimate is obtained using two processing steps. The first step involves an estimation of a coarse displacement estimate utilizing B-mode or envelope signals. To reduce computational time, the coarse displacement estimates are obtained starting from down-sampled B-mode pre- and post-compression image pairs using a pyramidal processing approach. The coarse displacement estimate obtained from the B-mode data is used to guide the final 2D cross-correlation computations on radio-frequency (RF) data. Results from finite element simulations and *in vivo* experimental data demonstrate the feasibility of this approach for imaging tissue with discontinuous displacement fields.

Introduction

Elastography and other elasticity imaging techniques provide imaging methods that are useful in the detection and characterization of stiffer areas such as tumours in breast, prostate, thyroid, liver (Bamber and Bush 1996, Fatemi and Greenleaf 1999, Hall *et al* 2003, Insana *et al* 2000, Levinson *et al* 1995, Nightingale *et al* 2002, O'Donnell *et al* 1994, Ophir *et al* 1991, Parker *et al* 1990, Talhami *et al* 1994, Wilson and Robinson 1982), characterization of the components of atherosclerotic plaque in both the coronary (de Korte *et al* 1997, 1998, 2000a, 2000b,

2002) and carotid arteries, and in the evaluation of cardiac function (Konofagou *et al* 2002, Varghese *et al* 2002) among other applications. In general for elasticity imaging approaches, a mechanical stimulus is applied to the tissue being imaged, and the resulting displacement and local strain estimated from the pre- and post-compression radio frequency (RF) data.

Many of the 2D algorithms developed for elasticity imaging assume continuity of the displacement field due to tissue continuity (Yeung *et al* 1998, Zhu and Hall 2002), which is a valid assumption in most tissue geometries. However, in certain imaging situations such as in the imaging of elasticity in the arteries, this assumption may not be valid for certain *in vivo* scanning geometries. Many researchers have applied elasticity imaging techniques for vessel wall imaging, with many of these applications focused on catheter based intravascular ultrasound (IVUS) elastography that utilizes the arterial pulsations as the mechanical stimuli (de Korte *et al* 1997, 1998, 2000a, 2000b, 2002). IVUS elastography is an invasive method, and the quality of the estimated local strain suffers from many artefacts such as reverberation ring artefacts, catheter motion during data acquisition, strain projection artefacts due to catheter position in vessel (De Korte *et al* 1999, Shi *et al* 2003, 2005). However, these methods do provide valuable information regarding the stiffness properties of the plaque within the vessel that is useful for the characterization of atherosclerotic plaque.

For shallower blood vessels such as the carotid artery, conventional ultrasound systems using higher frequency transducers are generally utilized to image the vessel wall for the evaluation of atherosclerotic plaque and need for surgical procedures such as carotid endarterectomy. Strain imaging can also be performed in shallower large arteries in a totally non-invasive manner utilizing the arterial pulsations as the mechanical stimuli. Since the ultrasound scanning performed is totally non-invasive, patients are more comfortable during the clinical scanning procedure. However, one of the issues associated with the longitudinal imaging of the carotid artery is that the arterial wall closest to the transducer moves towards the transducer, while the distal wall moves away from the transducer due to the arterial pulsations. Therefore for strain imaging of the carotid artery, since the displacement field is no longer continuous, multi-level processing as discussed in this paper is essential to provide a means for tracking these displacements.

Many different methods have been developed to compute local strains in tissue; however, most of these algorithms were developed for the imaging of continuous media (Alam *et al* 1998, Brusseau *et al* 2000, Chaturvedi *et al* 1998a, 1998b, O'Donnell *et al* 1994). Multiscale methods have also been utilized for elasticity imaging (Chaturvedi *et al* 1998a, Pellot-Barakat *et al* 2004). Zhu *et al* (1999) used a 2D deformable mesh method to estimate strain, which accommodates more general forms of tissue motion. Later, Zhu and Hall (2002) introduced a modified block matching method to obtain real-time strain images, based on the assumption that the displacement field is continuous in tissue, and utilize displacement estimates from shallower depths to predict the displacements at deeper depths in tissue. Maurice *et al* (2004) have developed a method for noninvasive vascular elastography to characterize the mechanical properties of superficial arteries using the Lagrangian speckle model for two-dimensional strain estimation (Maurice *et al* 2005).

In this paper, we demonstrate the feasibility of utilizing a multi-level cross-correlation based 2D strain estimation method that can be utilized to obtain strain images in situations where the displacement fields are not continuous. In the following sections, we will compare the performance of the multi-level approach to both 1D cross-correlation and 2D block matching techniques using finite element simulation models. *In vivo* experimental results on a section of the carotid artery that demonstrates the ability of the multi-level algorithm to track local displacements on the distal wall of the carotid artery are also presented.
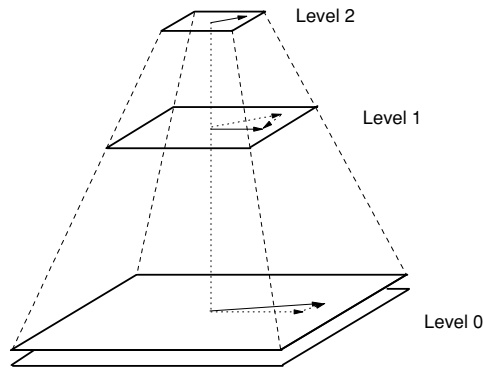
Figure 1. Schematic diagram of the multi-level motion tracking algorithm.

The multi-level algorithm

The multi-level pyramid construction for the elastographic processing of the pre- and post-compression frames is described in this section. Let L_{max} denote the total number of processing layers in the pyramid, where layer $L = 0$ is the bottom layer. In our application, the bottom layer ($L = 0$) is constructed from the RF data matrix. At the same time, a B-mode or envelope image B_0 from the RF data matrix is also generated. Layers $L = 1$ to $L_{max}-1$ are constructed with B-mode or envelope images. These B-mode images are generated by sub-sampling the initial B-mode image B_0 obtained from the $L = 0$ RF data matrix. For example, if we denote the B-mode image at layer L as B_L, B_L is a half sampled version of B_{L-1}. The reason that the layers $L = 1$ to $L_{max}-1$ are constructed with B-mode image data instead of directly down-sampling the RF data, is that direct down-sampling of RF data may violate the Nyquist sampling criterion. On the other hand, B-mode images are smoother (envelope of the RF signals) and down-sampling of the B-mode image would still maintain the B-mode features of the ultrasound image. The bottom layer $L = 0$ is constructed using the RF data matrix instead of the B-mode image since motion tracking on RF signals provides more precise displacement estimates. Figure 1 illustrates the multi-level pyramid constructed for the elastographic processing. Processing the ultrasound data in this manner enables the precise and high resolution estimation of the displacement on the RF frame pairs, since these are guided by the coarser displacement estimates obtained from the B-mode envelope data. The use of the multi-level pyramid in the processing of the B-mode data enables faster processing, and easier search and estimation of global displacement trends in the underlying tissue. This particular feature enables the accurate estimation of the displacement in discontinuous media such as in the elastographic imaging of arteries previously described, as opposed to most of the previously described techniques that assume continuity in the displacement estimates.

A 2D processing kernel is utilized for tracking the displacement due to the tissue deformation for all the stages of the multi-level pyramid proposed in this paper. Two-dimensional cross-correlation processing is used to track the displacement, with B-mode envelope signals used in levels $L = 1$ to $L_{max}-1$, and RF data for the $L = 0$ level. Since coarse displacement estimates are obtained from the B-mode envelope data, the final processing step on the RF data is conducted using 2D kernels whose sizes are around one wavelength in the axial dimension and 3–5 A-lines along the lateral or width direction.

The kernel size used at each level of the pyramid is independently set. Although we down-sample the envelope signals at each level, we still use larger kernels at the upper levels. The kernel size can be varied for different applications; for example, a combination of [15, 10], [4, 5], [1, 3] from the top to the bottom level was utilized in this paper, where the first value refers to the number of wavelengths utilized along the axial direction, while the second value denotes the number of A-lines used in the lateral direction.

The 2D cross-correlation coefficient which is used for the matching criteria or the confidence measure of the displacement estimate is shown below:

- For the $L = L_{max}-1$ (highest level):

$$CC(i, j) = \frac{\sum_{x=1}^{M}\sum_{y=1}^{N}[I_0(x, y) - \bar{I}_0][I_1(x + i, y + j) - \bar{I}_1]}{\sqrt{\sum_{x=1}^{M}\sum_{y=1}^{N}[I_0(x, y) - \bar{I}_0]^2 \times \sum_{x=1}^{M}\sum_{y=1}^{N}[I_1(x + i, y + j) - \bar{I}_1]^2}} \quad (1a)$$

- For the $L = L_{max} - 2$ to $L = 0$,

$$CC(i, j) = \frac{\sum_{x=1}^{M}\sum_{y=1}^{N}[I_0(x, y) - \bar{I}_0][I_1(x + i + i_0, y + j + j_0) - \bar{I}_1]}{\sqrt{\sum_{x=1}^{M}\sum_{y=1}^{N}[I_0(x, y) - \bar{I}_0]^2 \times \sum_{x=1}^{M}\sum_{y=1}^{N}[I_1(x + i + i_0, y + j + j_0) - \bar{I}_1]^2}}$$

$$(1b)$$

where I_0 and I_1 represent the pre- and post-compression data frames. i and j denote relative shifts between the I_0 and I_1 data frames in the same level, i_0 and j_0 are relative shifts between pre- and post-compression data frames from the upper layer. M and N are the block sizes in axial and lateral directions, where $\bar{I}_0$ and $\bar{I}_1$ denote the mean values of the blocks I_0 and I_1 used in calculation.

After motion or displacement tracking at each level of the pyramid, we utilize the normalized cross-correlation coefficient as a confidence measure corresponding to the reliability of the displacement estimate. Displacement estimates with a low normalized cross-correlation coefficient are replaced or interpolated from surrounding displacement estimates that possess a higher normalized cross-correlation value. The threshold for the normalized cross-correlation coefficients was empirically chosen. For example, for a pyramid with $L_{max} = 3$, we choose [0.3, 0.5, 0.6, 0.75] as the cross-correlation threshold for levels 3, 2, 1, 0 respectively.

Following displacement estimation, a cubic spline based smoothing technique is utilized to reduce noise artefacts, in the estimated displacement field $D_0(x, y)$. Assuming that $D_0(x, y)$ denotes the estimated displacement field, where x denotes the lateral direction, and y the axial direction, the function of the cubic spline smoothed displacement field $D_1(x, y)$ is to satisfy the following condition:

$$\underset{D_1(x,y)}{\arg\min} \sum_x \sum_y \left[p|D_0(x, y) - D_1(x, y)|^2 + (1 - p)\frac{d^2 D_1(x, y)}{dy^2} \right]. \quad (2)$$

The first term in the above bracket is utilized to keep the smoothed displacement field $D_1(x, y)$ close to the original estimated displacement field $D_0(x, y)$. The second term in the above bracket represents the second-order derivative of the smoothed displacement field $D_1(x, y)$. The weighting parameter p ($0 < p < 1$) is used to balance the contribution of these two terms to the smoothing of the displacement field. When $p = 1$, $D_1(x, y)$ becomes the least-squares straight line fit of the original displacement field $D_0(x, y)$. At the other extreme when $p = 0$, $D_1(x, y)$ becomes the natural cubic spline fit of the original displacement field $D_0(x, y)$. When the weighting parameter takes a value between 0 and 1 (i.e. $0 < p < 1$) the smoothed displacement field $D_1(x, y)$ lies between the least-squares straight line fit and natural cubic fit.

Simulation results

Method

To verify the performance of the 2D multi-level algorithm on discontinuous media, we utilize the commercial ANSYS finite element analysis (FEA) software to simulate the deformation induced by the pulsation of blood on simulated vessel walls embedded in tissue. Tissue with the embedded vessel was scanned using a linear array transducer with a width of 4 cm and an imaging depth of 5 cm. The vessel wall was simulated to have a thickness of 5 mm, and the inner diameter of the vessel was set to 5 mm. The modulus ratio for vessel wall versus the surrounding tissue was set at 2:1. The top and bottom boundaries of the tissue surrounding the vessel are fixed, and internal pressure perpendicular to the vessel wall applied from within the vessel lumen.

The pre-compression nodal positions and the displacement field after compression are then utilized in an ultrasound simulation program (Li and Zagzebski 1999) to generate pre- and post-compression RF echo signal data for elastographic processing. This program simulates the frequency domain response of ultrasound wave transmission through a scattering medium. The frequency response is then transformed back to the time domain to obtain ultrasound images. This simulation program achieves similar RF waveforms when compared to typical time domain simulation programs such as Field II. We simulate the speed of sound in tissue to be 1540 m s^{-1}, the size of scatterers as 50 μm and the density of scatterers to be 10^{11} m^{-3} to simulate Rayleigh scattering statistics. The simulated centre frequency is 10 MHz with 80% bandwidth. The region corresponding to blood flow, i.e. the region within the vessel lumen was not assigned any material properties in the ANSYS finite element simulation software. However, in the frequency domain ultrasound simulation program, this region with blood flow comprises random scatterers with a very low density (10^6 m^{-3}, which is $1/10^5$ of the scattering density in tissue) when compared to the scattering from surrounding tissue similar to that observed under *in vivo* scanning conditions. The backscattered signals from the region within the lumen are significantly lower in the RF pre- and post-compression signals, due to the lower density of the scatterers. The cross-correlation coefficient values in this region between the pre- and post-pressure signals are also quite low. We compare the performance of the following strain estimation algorithms to compute the elastograms or strain images from the simulated RF data pairs, namely the: (1) 1D cross-correlation method; (2) 2D block matching method that utilizes the continuity assumption; (3) 2D multi-level method.

Results

Figures 2(a) and (b) show the pre- and post-compression B-mode images. The simulated ideal strain image obtained using ANSYS is shown in figure 2(c), while figures 2(d)–(f) show the calculated elastogram using the three methods mentioned above. Note from figure 2(d) that the 1D cross-correlation method fails due to the increased lateral signal decorrelation due to the movement of the scatterers in the lateral direction. The 2D block matching method works well for the top half of the vessel as expected (see figure 2(e)), since the displacement field is continuous to that point. However, starting from the middle of the vessel, the displacement field becomes discontinuous, since the tissue displacement in this region is away from the transducer as opposed to the first half of the vessel where the displacement is towards the transducer. Therefore this method fails, as would all the methods developed for continuous media (where the displacement field is continuous) since they are unable to track these discontinuous displacement fields. The strain image or elastogram obtained for the lower half
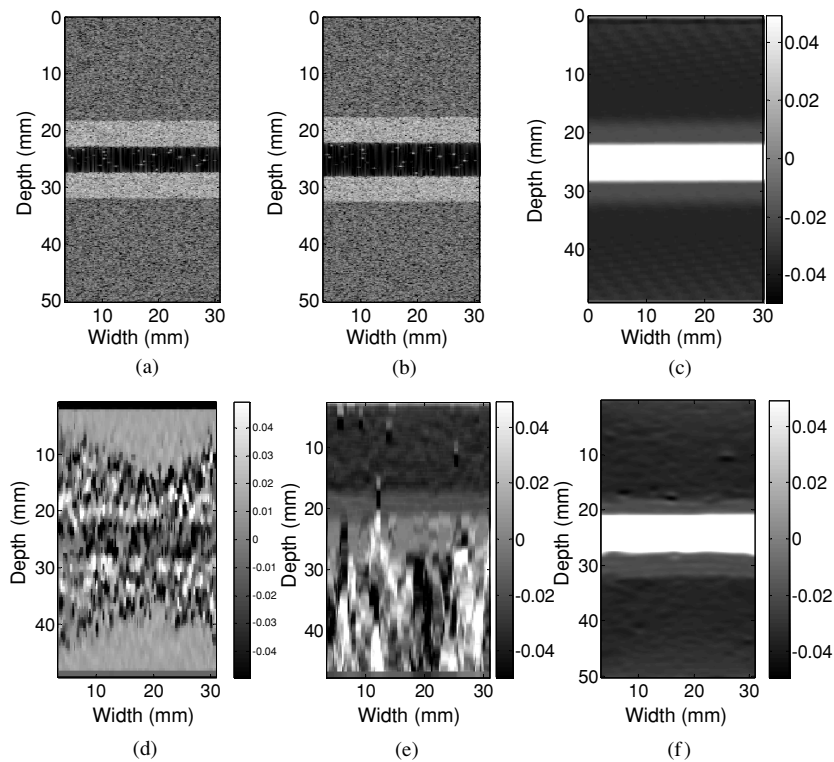
Figure 2. Ultrasound B-mode and strain images for a simulated artery. B-mode images (a) before and (b) after the internal applied pressure within the lumen to deform the artery walls. The ideal axial strain image obtained using the ANSYS model (c). Local strain images obtained using (d) 1D cross-correlation (e) 2D block matching, and (f) the 2D multi-level method.

is therefore contaminated with increased noise artefacts. On the other hand, the 2D multi-level method tracks the displacement field accurately, and the calculated elastogram clearly shows the vessel wall on both sides of the lumen. The 2D multi-level algorithm does not make any assumptions regarding the continuity of the displacement field. Comparing figure 2(f) with the ANSYS simulated strain result shown in figure 2(c) illustrates the similarity in the results.

A quantitative comparison of the strain estimation performance of the 2D multi-level method with the 2D block matching method is illustrated in figure 3. Figure 3(a) presents plots of the variation in the signal-to-noise ratio (SNR_e) in a uniformly elastic region around the top edge of the vessel phantom at different compressions. We choose a region of interest (ROI) with dimensions of 1 cm^2 centred at depth of 1 cm. Observe that the SNR_e values obtained for 2D block matching for small compression (1–2%) are higher than the 2D multi-level method, while at larger applied compressions, the SNR_e for both methods are very similar. This result compares the performance of the two 2D methods in media where the displacement field is continuous. The primary reason for the better performance of the 2D block matching method is due to the fact that it tracks the displacement by utilizing *a priori* displacement information from the previous row, and therefore for small strains the displacement field satisfies the continuity assumption due to the smooth displacement field. The 2D multi-level algorithm, on the other hand, estimates the displacement field at each location, and thus the neighbouring displacement estimates could be discontinuous, and therefore the strain estimated from the displacement field has a smaller SNR_e than the 2D block matching approach.
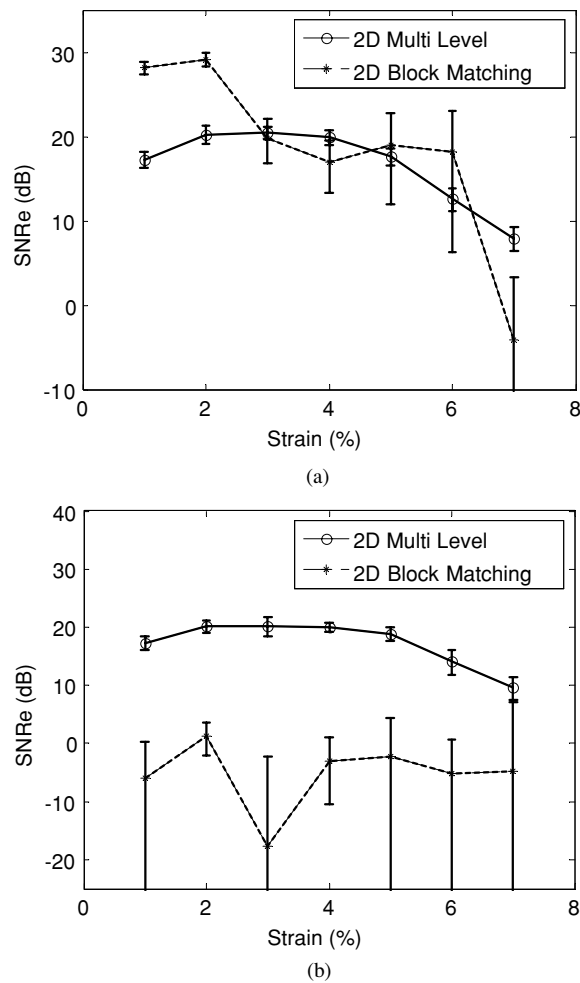
Figure 3. Comparison of the SNR_e obtained versus applied strain for the 2D multi-level method and block matching methods, for a 1 cm^2 region (a) centred at depth of 10 mm depth; (b) and centred at a depth of 40 mm (after the distal wall).

The 2D multi-level method, however, performs better for discontinuous media such as for blood vessels, where the displacement field is discontinuous starting at the vessel lumen. The improvement in the strain estimation performance is illustrated in figure 3, where the variations in the SNR_e are plotted for ROIs within the vessel wall on the proximal side in figure 3(a), and the distal side in figure 3(b). Note that the multi-level method performs significantly better than the block-matching method on the distal part of the vessel as illustrated in figure 3(b).

Simulation results obtained using a FEA simulation of a fibrous capsule with a lipid inclusion are shown in figure 4. Plaque geometry within a typical carotid artery is simulated and meshed using ANSYS. The model shows a lipid based plaque with a thin fibrous capsule surrounding the lipid region attached to the bottom wall of the artery. A small calcified region is also simulated inside the lipid region. The deformation of the plaque is obtained by applying a uniform pressure from within the lumen similar to that utilized in figure 2, on both the inner wall and the plaque capsule. The resultant displacement field as well as the initial nodal position of the mesh is then utilized by the ultrasound simulation program to generate pre- and
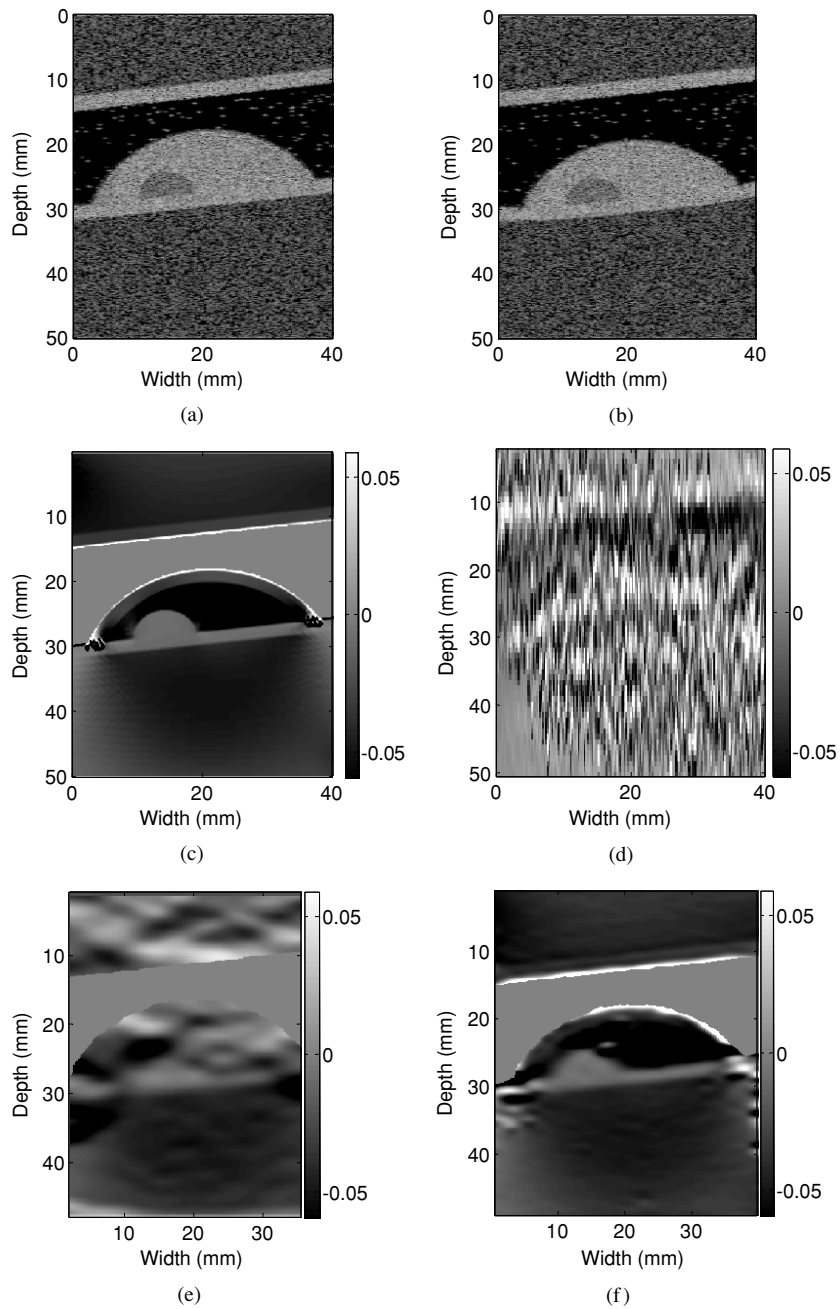
(a)

(b)

(c)

(d)

(e)

(f)

Figure 4. Ultrasound B-mode and strain images for a simulated artery with atherosclerotic plaque. (a) B-mode image before and (b) after compression, and the (c) ideal strain image obtained using FEA analysis. Local strain images obtained using (d) 1D cross-correlation, (e) 2D block matching and (f) the 2D multi-level method.

post-compression RF data frames. Figures 4(a) and (b) show the B-mode images before and after compression, while figure 4(c) shows the ideal strain image calculated from the ANSYS displacement field.

Elastograms or axial strain images are then calculated using 1D cross-correlation, 2D block matching and the 2D multi-level method. Figure 4(d) shows the strain image obtained using 1D cross-correlation, and figure 4(e) presents results from the 2D block matching algorithm. The strain image calculated using the 2D multi-level method is shown in figure 4(f), where the plaque structure simulated is clearly observed as simulated using the FEA, when compared to figure 4(c). In a similar manner as was illustrated in figure 2, 1D cross-correlation fails due to the increased lateral motion of the scatterers, while the 2D block-matching algorithm estimates the local displacement field up to the lumen centre or as long as the displacement field is continuous. In figure 4(e) for the block-matching algorithm, displacements were computed from the distal end of the artery, such that simulated tissue that included the plaque was continuous. This is the reason for the noise artefacts in the top section of the strain image in figure 4(e).

Experimental results

Experimental setup and data processing

In vivo data acquisition on patients with carotid stenosis and plaque was performed at the University of Wisconsin-Madison Hospitals and Clinics. This study was approved by the UW-Madison Institutional Review Board (IRB) for data acquisition on human patients. Ultrasound RF data were acquired on patients who had consented to the study, using a Siemens Antares system with the Axius direct ultrasound research interface (URI). Patient scanning was performed as a standard clinical carotid examination, where the sonographer places the VFX 13-5 transducer on the skin surface at the location of carotid artery. The centre frequency of the transducer was set at the highest frequency of the transducer, i.e., 11.43 MHz. The lateral resolution was also set to the highest value, i.e. 508 A-lines for a beamwidth of 38 mm. The sampling rate was 40 MHz, and a single transmit focus was set at the depth of the plaque with dynamic focusing on receive. Radiofrequency data were acquired at the maximum frame rate allowed by the system under the imaging conditions described above. During data acquisition, the patients were requested to hold their breath to reduce respiratory motion artefacts. After data acquisition on the patient, RF data were transferred to a personal computer for off-line post-processing. Normalized 2D cross-correlation processing was performed on RF data frames with a relative deformation of around 1–2% to compute the displacement field and local strain using the multi-level processing technique described in the paper.

Figures 5(a) and (b) show typical pre- and post-deformation B mode images from a patient prior to carotid endarterectomy. The ultrasound B-mode images show a large plaque attached to the distal wall of the carotid artery. The plaque contains both soft region and calcified regions that are clearly seen using the arrows. The arrow at the bottom points to the location of the calcified region, while the five arrows at the top indicate the boundary of the plaque. The softer plaque region is under the top three arrows on the right. We expect a relatively low strain area on elastogram, corresponding to the calcified region, and a relatively high strain region corresponding to the softer region. We also expect to be able to visualize the plaque boundaries on the elastogram.

Figures 5(c) and (d) show the elastograms calculated using 1D cross-correlation, and the 2D block matching method respectively. Observe from figure 5(c) that the 1D cross-correlation method does not perform well at the plaque boundary due to increased lateral signal decorrelation. In figure 5(d), the strain image obtained using 2D block-matching based on the tissue continuity assumption provides accurate estimation of local strain for regions
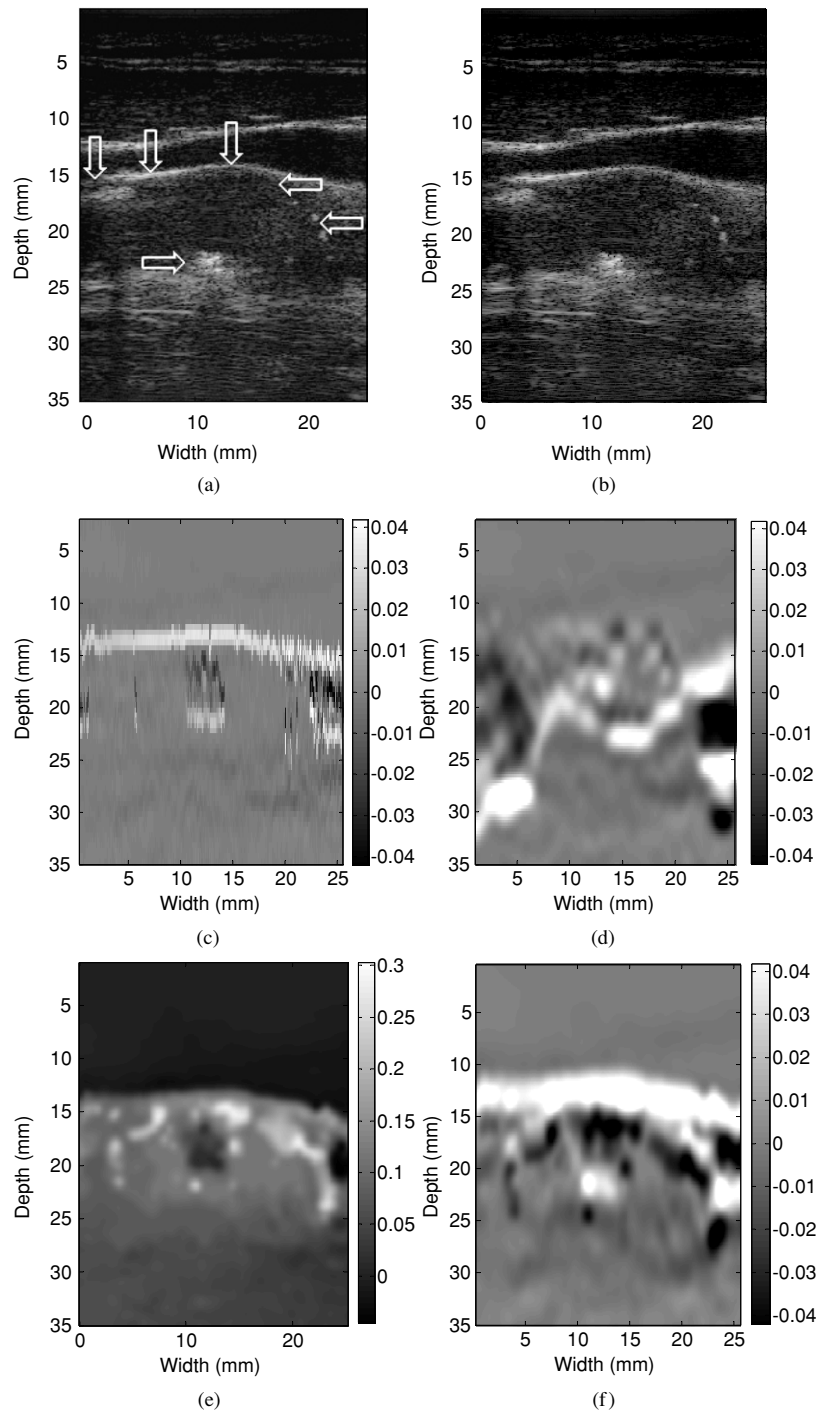
Figure 5. Ultrasound B-mode and strain images for an *in vivo* carotid artery with atherosclerotic plaque. (a) B-mode image before (frame 43) and (b) after (frame 44) the deformation induced by the blood flow. Local strain images obtained using (c) 1D cross-correlation and the (d) 2D block matching method. Both the local (e) displacement field and (f) strain image calculated using the 2D multi-level method are presented.

near the vessel wall closest to the transducer, and fails to estimate local displacements from the vessel boundary distal to the transducer (since the tissue continuity assumption does not hold in this region). On the other hand, figure 5(e) presents the local displacement field estimated using the 2D multi-level method described in this paper. Figure 5(e) shows that the displacement field becomes discontinuous almost immediately at locations close to the artery wall closest to the transducer. Finally, figure 5(f) presents the local strain image generated from displacement image shown in figure 5(e), obtained using the 2D multi-level algorithm.

Observe from figure 5(f) that the boundary of the plaque is clearly delineated in the elastogram, while on the B-mode images 5(a), (b) the boundary is not clearly visualized. Moreover, the elastogram in figure 5(f) shows large regions inside the plaque that exhibit uniform strains. A region that incurs large strains, indicating a softer region is also clearly visualized. We have to point out that the large strain region does not represent the calcified region; instead, it is located just above the calcified region. The strain value corresponding to the calcified region is actually close to zero. The elastogram shown in figure 5(f) correlates very well with the B-mode image, as well as providing useful information not obtained from the B-mode image (figure 5(a)).

Discussion

In this paper, we demonstrate the ability of the 2D multi-level cross-correlation method to compute local displacement fields and strains in discontinuous media. Coarse displacement estimates are initially obtained using sub-sampled B-mode data using a multi-level pyramid algorithm. The coarse displacement estimates are then utilized to guide the high resolution estimation on the lowest level of the pyramid containing the RF echo signal data. This method combines the advantages provided by the robustness of B-mode envelope tracking and the precision obtained using RF motion tracking to obtain high resolution displacement and strain estimates. The processing scheme described in this paper that utilizes the coarse displacement estimation using B-mode data and the multi-level approach enables the algorithm to track discontinuous displacement fields. This algorithm is therefore not limited by the assumption of a continuous displacement field utilized in most strain estimation algorithms. This method therefore is particularly suited for local strain estimation of blood vessels and for plaque characterization.

Several groups (Yeung *et al* 1998) have applied speckle tracking algorithms by searching regions using larger 2D search regions over the B-mode images and progressively moving to smaller blocks to improve the resolution of the strain image. The approach followed by Yeung *et al* (1998), however, does not down-sample the ultrasound B-mode image to construct the multi-level pyramid, claiming that the down-sampling of the B-mode images would change the speckle patterns. However, in our multi-level method, we find that the down-sampling of the B-mode images does not introduce any speckle tracking problems. In contrast, the smaller B-mode image sizes in each upper level of the pyramid significantly improve the computational efficiency.

Maurice *et al* (2004) developed a method for noninvasive vascular elastography, using the Lagrangian speckle model to estimate two-dimensional tissue motion. This estimator iteratively optimizes the motion field between pre- and post-compression images to obtain an optimum match. However, this approach has the drawback that the calculation of motion relies on the model, which has been evaluated in simulations. However for *in vivo* applications, tissue motion is complicated and the appropriate tissue motion model may be difficult to set up. In addition, the assumption regarding the linear transformation between the pre- and

post-compression data would be dependent on specific strain imaging applications and may be restrictive in certain situations.

Pellot-Barakat *et al* (2004) have also utilized a multiscale method to track tissue displacements. However, they assume tissue continuity which is different from our approach as previously described. In their *in vitro* experiment, the ultrasound transducer is placed on the top surface of the phantom, and the induced displacement field after compression with the transducer is primarily along the same direction. This differs from the results reported in this paper where pressure is applied within the lumen, and the displacement fields are in opposite directions, i.e. towards the transducer before the lumen and away from the transducer beyond the lumen.

In this paper, we focus on strain estimation in discontinuous tissue or tissue with discontinuous motion fields. Smoothing of the displacement field after displacement estimation in each level using the cubic splines reduces errors in propagation of the displacement estimates at each level. The selection of the value of the weighting parameter '*p*' is important for estimation of the local displacement fields. When the weighting parameter approaches 0, the displacement field obtained is similar to that obtained using the linear least-squares fit of the displacement field, while when the weighting parameter is close to 1, the displacement field is the same as the natural cubic spline fit of the original displacement field.

To compare the computational load, we ran the three algorithms in the same environment, i.e., Matlab 7.0 on a PC (Windows XP Pro, Pentium III 1GB CPU, 512MB memory). For a typical data set with 4096 points along the axial direction and 360 A-lines, the computation time for the 1D cross-correlation algorithm was $\sim$30 s (this value varies depending on the CPU fraction), while the typical computation time for the Matlab code for the 2D block matching algorithm requires $\sim$9 times the computation time, while the Matlab code with the multi-level algorithm requires $\sim$14 times the computational time. One of the reasons why the 2D multi-level code is more computationally intensive is due to the large search range in the upper levels to obtain the relative movement between the two frames. However, these codes can be rewritten using C++; and run on a faster state-of-the-art system to improve computational efficiency and operate in real time.

Conclusion

In this paper, we explore the feasibility of utilizing a 2D multi-level cross-correlation based method to compute local displacements and strains for discontinuous tissue. The FEA simulations and *in vivo* experimental data demonstrate the improvement in the strain estimation performance over algorithms based on the tissue continuity assumption.

Acknowledgment

References

Alam S K, Ophir J and Konofagou E E 1998 An adaptive strain estimator for elastography *IEEE Trans. Ultrason. Ferroelectr. Freq. Control* **45** 461–72

Bamber J C and Bush N L 1996 Freehand elasticity imaging using speckle decorrelation rate *Acoust. Imaging* **22** 285–92

Brusseau E, Perrey C, Delachartre P, Vogt M, Vray D and Ermert H 2000 Axial strain imaging using a local estimation of the scaling factor from RF ultrasound signals *Ultrason. Imaging* **22** 95–107

Chaturvedi P, Insana M F and Hall T J 1998a 2-D companding for noise reduction in strain imaging *IEEE Trans. Ultrason. Ferroelectr. Freq. Control* **45** 179–91

Chaturvedi P, Insana M F and Hall T J 1998b Testing the limitations of 2-D companding for strain imaging using phantoms *IEEE Trans. Ultrason. Ferroelectr. Freq. Control* **45** 1022–31

De Korte C L, Cespedes E I and Van Der Steen A F W 1999 Influence of catheter position on estimated strain in intravascular elastography *IEEE Trans. Ultrason. Ferroelectr. Freq. Control* **46** 616–25

de Korte C L, Cespedes E I, van Der Steen A F and Lancee C T 1997 Intravascular elasticity imaging using ultrasound: feasibility studies in phantoms *Ultrasound Med. Biol.* **23** 735–46

de Korte C L, Pasterkamp G, van Der Steen A F, Woutman H A and Bom N 2000a Characterization of plaque components with intravascular ultrasound elastography in human femoral and coronary arteries in vitro *Circulation* **102** 617–23

de Korte C L, Sierevogel M J, Mastik F, Strijder C, Schaar J A, Velema E, Pasterkamp G, Serruys P W and van Der Steen A F 2002 Identification of atherosclerotic plaque components with intravascular ultrasound elastography *in vivo*: a Yucatan pig study *Circulation* **105** 1627–30

de Korte C L, van Der Steen A F, Cepedes E I, Pasterkamp G, Carlier S G, Mastik F, Schoneveld A H, Serruys P W and Bom N 2000b Characterization of plaque components and vulnerability with intravascular ultrasound elastography *Phys. Med. Biol.* **45** 1465–75

de Korte C L, van Der Steen A F, Cespedes E I and Pasterkamp G 1998 Intravascular ultrasound elastography in human arteries: initial experience *in vitro Ultrasound Med. Biol.* **24** 401–8

Fatemi M and Greenleaf J F 1999 Application of radiation force in noncontact measurement of the elastic parameters *Ultrason. Imaging* **21** 147–54

Hall T J, Zhu Y and Spalding C S 2003 *In vivo* real-time freehand palpation imaging *Ultrasound Med. Biol.* **29** 427–35

Insana M F, Cook L T, Bilgen M, Chaturvedi P and Zhu Y 2000 Maximum-likelihood approach to strain imaging using ultrasound *J. Acoust. Soc. Am.* **107** 1421–34

Konofagou E E, D'Hooge J and Ophir J 2002 Myocardial elastography–a feasibility study *in vivo Ultrasound Med. Biol.* **28** 475–82

Levinson S F, Shinagawa M and Sato T 1995 Sonoelastic determination of human skeletal muscle elasticity *J. Biomech.* **28** 1145–54

Maurice R L, Brusseau E, Finet G and Cloutier G 2005 On the potential of the Lagrangian speckle model estimator to characterize atherosclerotic plaques in endovascular elastography: *in vitro* experiments using an excised human carotid artery *Ultrasound Med. Biol.* **31** 85–91

Maurice R L, Ohayon J, Fretigny Y, Bertrand M, Soulez G and Cloutier G 2004 Noninvasive vascular elastography: theoretical framework *IEEE Trans. Med. Imaging* **23** 164–80

Nightingale K, Soo M S, Nightingale R and Trahey G 2002 Acoustic radiation force impulse imaging: *in vivo* demonstration of clinical feasibility *Ultrasound Med. Biol.* **28** 227–35

O'Donnell M, Skovoroda A R, Shapo B M and Emelianov S Y 1994 Internal displacement and strain imaging using ultrasonic speckle tracking *IEEE Trans. Ultrason. Ferroelectr. Freq. Control* **41** 314–25

Ophir J, Cespedes I, Ponnekanti H, Yazdi Y and Li X 1991 Elastography: a quantitative method for imaging the elasticity of biological tissues *Ultrason. Imaging* **13** 111–34

Parker K J, Huang S R, Musulin R A and Lerner R M 1990 Tissue response to mechanical vibrations for 'sonoelasticity imaging' *Ultrasound Med. Biol.* **16** 241–6

Pellot-Barakat C, Frouin F, Insana M F and Herment A 2004 Ultrasound elastography based on multiscale estimations of regularized displacement fields *IEEE Trans. Med. Imaging* **23** 153–63

Shi H, Chen Q and Varghese T 2005 A general solution for catheter position effects for strain estimation in intravascular elastography *Ultrasound Med. Biol.* **31** 1509–26

Shi H, Varghese T, Chen Q and Gimelli G 2003 correction for catheter eccentricity and tilt in intravascular elastography *Ultrason. Imaging* **25** 262–83

Talhami H E, Wilson L S and Neale M L 1994 Spectral tissue strain: a new technique for imaging tissue strain using intravascular ultrasound *Ultrasound Med. Biol.* **20** 759–72

Varghese T, Zagzebski J A, Rahko P, Douglas P S and Breburda C S 2002 Cardiac elastography: a novel method for real-time 2-D strain imaging (abstract) *J. Ultrasound Med.* **21** S44

Wilson L S and Robinson D E 1982 Ultrasonic measurement of small displacements and deformations of tissue *Ultrason. Imaging* **4** 71–82

Yeung F, Levinson S F and Parker K J 1998 Multilevel and motion model-based ultrasonic speckle tracking algorithms *Ultrasound Med. Biol.* **24** 427–41

Zhu Y, Chaturvedi P and Insana M F 1999 Strain imaging with a deformable mesh *Ultrason. Imaging* **21** 127–46

Zhu Y and Hall T J 2002 A modified block matching method for real-time freehand strain imaging *Ultrason. Imaging* **24** 161–76